A New Manganese Dinuclear Complex with Phenolate Ligands and a Single Unsupported Oxo Bridge. Storage of Two Positive Charges within Less than 500 mV. Relevance to Photosynthesis

Olivier Horner,[†,§] Elodie Anxolabéhère-Mallart,[†] Marie-France Charlot,[†] Lyuba Tchertanov,[‡] Jean Guilhem,[‡] Tony A. Mattioli,[¶] Alain Boussac,[§] and Jean-Jacques Girerd*[,†]

Laboratoire de Chimie Inorganique, URA CNRS 420, Université de Paris-Sud, 91405 Orsay, France, Laboratoire de Cristallochimie, Institut de Chimie des Substances Naturelles, 91198 Gif-sur-Yvette, France, Section de Bioenergétique, URA CNRS 2096, DBCM, CEA Saclay, 91191 Gif-sur-Yvette, France, and Section de Biophysique des Protéines et des Membranes, URA CNRS 2096, DBCM, CEA Saclay, 91191 Gif-sur-Yvette, France

Received July 17, 1998

The compound $[Mn^{III}_2OL_2](ClO_4)_2.2.23CHCl_3.0.65CH_2Cl_2$ where L^- is the monoanionic *N*,*N*-bis(2-pyridylmethyl)-*N*′-salicyliden-1,2-diaminoethane ligand, has been synthesized. The complex dication $[Mn^{III}_2OL_2]^{2+}$ contains a linear Mn(III)−O−Mn(III) unit with a Mn−Mn distance of 3.516 Å. The pentadentate ligand L^- wraps around the Mn(III) ion. Electrochemically, it is possible to prepare the one electron oxidized trication $[Mn_2OL_2]^{3+}$ which crystallizes as $[Mn_2OL_2](ClO_4)_{2.37}(PF_6)_{0.63}\cdot 1.5CH_3CN$. The complex trication $[Mn_2OL_2]^{3+}$ contains a Mn(III)−O−Mn(IV) unit with a Mn−Mn distance of 3.524 Å and a Mn−O−Mn angle of 178.7(2)°. The contraction of the coordination sphere around the Mn(IV) is clearly observed. The $[Mn_2OL_2]^{2+}$ dication possesses a $S = 0$ electronic ground state with $J = -216$ cm^{-1} ($H = -J\mathbf{S_1}\cdot\mathbf{S_2}$), whereas the $[Mn_2OL_2]^{3+}$ trication shows a $S = {}^1/_2$ ground state with $J = -353$ cm^{-1}. The UV−visible spectrum of $[Mn_2OL_2]^{3+}$ exhibits an intense absorption band ($\epsilon = 3040$ M^{-1} cm^{-1}) centered at 570 nm assigned to a phenolate → Mn(IV) charge-transfer transition. The potentials of the redox couples determined by cyclic voltammetry are $E°$ ($[Mn_2OL_2]^{3+}/[Mn_2OL_2]^{2+}$) = 0.54 V/saturated calomel electrode (SCE) and $E°$ ($[Mn_2OL_2]^{4+}/[Mn_2OL_2]^{3+}$) = 0.99 V/SCE. Upon oxidation at 1.3 V/SCE, the band at 570 nm shifts to 710 nm ($\epsilon = 2500$ M^{-1} cm^{-1}) and a well-defined band appears at 400 nm which suggests the formation of a phenoxyl radical. The $[Mn_2OL_2]^{3+}$ complex exhibits a 18-line X-band electron paramagnetic resonance (EPR) spectrum which has been simulated with rhombic tensors $|A_{1x}| = 160 \times 10^{-4}$ cm^{-1}; $|A_{1y}| = 130 \times 10^{-4}$ cm^{-1}; $|A_{1z}| = 91 \times 10^{-4}$ cm^{-1}; $|A_{2x}| = 62 \times 10^{-4}$ cm^{-1}; $|A_{2y}| = 59 \times 10^{-4}$ cm^{-1}; $|A_{2z}| = 62 \times 10^{-4}$ cm^{-1} and $g_x = 2.006$; $g_y = 1.997$; $g_z = 1.982$. This EPR spectrum shows that the 16-line paradigm related to a large antiferromagnetic exchange coupling and a low anisotropy can be overcome by a large rhombic anisotropy. Molecular orbital calculations relate this rhombicity to the nature of the orbital describing the extra electron on Mn(III). This orbital has a majority but not pure d_{z^2} contribution (with the *z* axis perpendicular to the Mn−Mn axis). Low-temperature resonance Raman spectroscopy on an acetonitrile solution of $[Mn_2OL_2]^{4+}$ prepared at −35 °C indicated the formation of a phenoxyl radical. This suggests that the ligand was oxidized rather than the Mn(III)Mn(IV) pair to Mn(IV)Mn(IV), which illustrates the difficulty to store a second positive charge in a short range of potential in a manganese mono-μ-oxo pair. The relevance of these results to the study of the photosynthetic oxygen evolving complex is discussed.

Introduction

Photosystem II (PS II) carries out photochemical extraction of electrons from water, forming molecular oxygen following the equation

$$2H_2O \rightarrow O_2 + 4H^+ + 4e^-$$

The catalytic center for this essential four-electron oxidation reaction is known as the oxygen evolving complex (OEC). It contains a cluster of four Mn ions cycling through five oxidation states, S_0 to S_4, the index referring to the number of oxidizing equivalents stored.[1,2] Oxygen is released during the S_3 to S_0 step in which S_4 is a transient state. The S_2 state is characterized by a multiline electron paramagnetic resonance (EPR) signal[3] which arises from an $S = {}^1/_2$ ground state.[4] The ligands of the Mn cluster have not yet been fully identified even though the coupling of the Mn to imidazole nitrogens has been observed.[5]

[†] Laboratoire de Chimie Inorganique.
[‡] Laboratoire de Cristallochimie.
[§] Section de Bioenergétique.
[¶] Section de Biophysique des Protéines et des Membranes.

(1) For reviews, see: Debus, R. J. *Biochim. Biophys. Acta* **1992**, *1102*, 269−352. Rutherford, A. W.; Zimmerman, J.-L.; Boussac, A. In *The Photosystems: Structure, Function and Molecular Biology*; Barber, J., Ed.; Elsevier Science Publisher: New York, 1992, Chapter 5, pp 179−229.
(2) Yachandra, V. K.; Sauer, K.; Klein, M. P. *Chem. Rev.* **1996**, *96*, 2927−2950.
(3) Dismukes, G. C.; Siderer, Y. *Proc. Natl. Acad. Sci. U.S.A.* **1981**, *78*, 274−278.
(4) Britt, R. D.; Lorigan, G. A.; Sauer, K.; Klein, M. P.; Zimmerman, J.-L. *Biochim. Biophys. Acta* **1983**, *1040*, 95−101.
(5) Tang, X. S.; Diner, B. A.; Larsen, B. S.; Gilchrist, M. L., Jr.; Britt, R. D.; Lorigan, G. A. *Proc. Natl. Acad. Sci. U.S.A.* **1994**, *91*, 704−708.

10.1021/ic980832m CCC: $18.00
Published on Web 03/04/1999

A broad radical EPR signal has also been detected in the S_3 state of Ca-depleted PS II.[6] Boussac et al.[7,8] have shown that this signal is related to the interaction between the Mn cluster in a redox state analogous to that in the S_2 state and a radical. The conclusive assignment of this radical to the tyrosyl radical Y_Z° was provided by ESEEM experiments.[9] A Mn−Y_Z° distance from 3.5 to 4.5 Å has been proposed in certain models.[10,11] This S_3 EPR signal is observed in perturbed systems in which the electron transfer between the Mn cluster and Y_Z° would be inhibited. The possibility of a close proximity between Y_Z° and the Mn cluster has stimulated the idea of an active role of Y_Z in the water oxidation process. Tyrosine Y_Z would be implied in electron−proton[10,11] or hydrogen transfer,[12−14] from a water molecule bound to Mn. This was considered feasible from model complexes data by Caudle and Pecoraro.[15]

The finding that Mn-tyrosine interaction may play a central role in water oxidation led us to focus our efforts on the synthesis of new Mn complexes containing phenolate ligands with the aim of studying their redox chemistry. Schiff-base type of ligands containing two phenol groups have given rise to a rich Mn chemistry.[16] For instance the ligand salpn[17] has allowed the preparation of [Mn(IV)(μ-O)$_2$Mn(IV)] complexes exhibiting interesting protonation chemistry of the oxo bridges.[18] Recently, mononuclear metal complexes containing the phenoxyl radical have been reported.[19−23] It is worthwhile to examine the possibility of the existence of such a species in the presence of a manganese polynuclear complex.

Electronic properties of Mn(III)−O−Mn(III), Mn(III)−O−Mn(IV), and Mn(IV)−O−Mn(IV) linear units are also of interest. In particular, because the discovery of ferromagnetic interaction in the Mn(III)−O−Mn(IV) unit in manganites $La_{1-x}Ca_xMn^{III}_{1-x}Mn^{IV}_xO_3$ [24] is at the origin of the double-exchange theory by Anderson and Hasegawa,[25] the synthesis of a molecular Mn(III)−O−Mn(IV) analogue is certainly a valuable goal to understand the mixed-valence properties of such a unit. Manganites are the object of intense studies by researchers in solid-state physics and chemistry.[26] A complex between the linear Mn(III)−O−Mn(III) unit and 5-NO_2saldien, a Schiff-base type of ligand with two phenol groups, has already been prepared.[27] Only a few other examples of dinuclear complexes in which Mn(III) atoms are bridged by a single oxo group are known.[28−30] To our knowledge no X-ray structure of a Mn(III)−O−Mn(IV) unsupported bridged system has been reported previously. A linear Mn(IV)−O−Mn(IV) has been characterized structurally in $[N_3Mn^{IV}(TPP)]_2O$.[31]

We report here the synthesis of the $[Mn^{III}_2OL_2]^{2+}$ complex in which $L^- = N,N$-bis(2-pyridylmethyl)-N'-salicylidene-ethane-1,2-diamine is the monoanionic pentadentate ligand represented below:

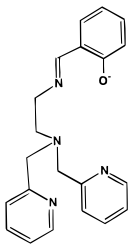

This ligand wraps around Mn(III), and the sixth coordination site is occupied by the bridging oxo group. We showed that this complex can be oxidized twice to successively give the $[Mn_2OL_2]^{3+}$ and $[Mn_2OL_2]^{4+}$ complexes. The structural characterization and the study of the electronic properties of the $[Mn^{III}_2OL_2]^{2+}$ and $[Mn^{III,IV}_2OL_2]^{3+}$ complexes are reported. Furthermore the $[Mn_2OL_2]^{4+}$ species was prepared electrochemically and was characterized by UV−vis and resonance Raman spectroscopies as a phenoxyl-radical containing $[Mn^{III,IV}_2$-$OLL^\circ]^{4+}$ species. These results show that a Mn(IV) ion and a phenoxyl radical can be close in energy and therefore in redox competition.

Experimental Section

Synthesis. All chemical syntheses were performed using Aldrich starting materials as received. The ligand *N*,*N*-bis(2-pyridylmethyl)-amine was prepared by following a reported procedure.[32] NMR spectra were recorded on a Bruker AC200 and AC250 spectrometer.

Caution! *Perchlorate salts of compounds containing organic ligands are potentially explosive. Only small quantities of these compounds should be prepared and handled behind suitable protective shields.*

For electrochemical experiments, tetraethylammonium perchlorate (Fluka) used as supporting electrolyte was recrystallized in ethanol 95%

(6) Boussac, A.; Zimmerman, J.-L.; Rutherford, A. W. *Biochemistry* **1989**, *28*, 8984−8989.
(7) Boussac, A.; Zimmerman, J.-L.; Rutherford, A. W.; Lavergne, J. *Nature* **1990**, *347*, 303−306.
(8) Boussac, B. *Biochim. Biophys. Acta* **1996**, *1277*, 253−265.
(9) Tang, X.-S.; Randall, D. W.; Force, D. A.; Diner, B. A.; Britt, R. D. *J. Am. Chem. Soc.* **1996**, *118*, 7638−7639.
(10) Gilchrist, M. L., Jr.; Ball, J. A.; Randall, D. W.; Britt, R. D. *Proc. Natl. Acad. Sci. U.S.A.* **1995**, *92*, 9545−9549.
(11) Force, D. A.; Randall, D. W.; Britt, R. D. *Biochemistry* **1997**, *36*, 12062−12070.
(12) Tommos, C.; Tang, X.-S.; Warncke, K.; Hoganson, C. W.; Styring, S.; McCracken, J.; Diner, B. A.; Babcock, G. T. *J. Am. Chem. Soc.* **1995**, *117*, 10325−10335.
(13) Tommos, C.; Babcock, G. T. *Acc. Chem. Res.* **1998**, *31*, 18−25.
(14) Hoganson, C. W.; Babcock, G. T. *Science* **1997**, *277*, 1953−1956.
(15) Caudle, M. T.; Pecoraro, V. L. *J. Am. Chem. Soc.* **1997**, *119*, 3415−3416.
(16) Wieghardt, K. *Angew. Chem., Int. Ed. Engl.* **1989**, *28*, 8, 1153−1172.
(17) Abbrevations used in the text: salpn^{2-}, *N*,*N*′-bis(salicylidene)propane-1,3-diamine dianion; 5-NO_2saldien^{2-}, *N*,*N*′-bis(5-nitrosalicylidene)-1,7-diamino-3-azapentane dianion; tphpn$^-$, tetrakis(2-methylpyridyl)-2-hydroxypropane-1,3-diamine monoanion; TACN, 1,4,7-triazacyclononane; bpy, 2-2′-bipyridine; phthal^{2-}, phthalocyanine dianion; py, pyridine; TPP^{2-}, tetraphenylporphyrine dianion; cat^{2-}, catecholate dianion; bispicen, *N*,*N*′-bis(2-pyridylmethyl)ethane-1,2-diamine; bispicMe_2-en, *N*,*N*′-dimethyl-*N*,*N*′-bis(2-pyridylmethyl)ethane-1,2-diamine.
(18) Baldwin, M. J.; Stemmler, T. L.; Riggs-Gelasco, P. J.; Kirk, M. L.; Penner-Hahn, J. E.; Pecoraro, V. L. *J. Am. Chem. Soc.* **1994**, *116*, 11349−11356.
(19) Adam, B.; Bill, E.; Bothe, E.; Goerdt, B.; Haselhorst, G.; Hildenbrand, K.; Sokolowski, A.; Steenken, S.; Weyhermüller, T.; Wieghardt K. *Chem. Eur. J.* **1997**, *3*, 308−313.
(20) Sokolowski, A., Müller, J.; Weyhermüller, T.; Schnepf, R.; Hildebrandt, P.; Hildenbrand, K.; Bothe, E.; Wieghardt, K. *J. Am. Chem. Soc.* **1997**, *119*, 8889−8900.
(21) Goldberg, D. P.; Watton, S. P.; Maschelein, A.; Wimmer, L.; Lippard, S. J. *J. Am. Chem. Soc.* **1993**, *115*, 5346.
(22) Halfen, J. A.; Jazdzewski, B. A.; Mahapatra, S.; Berreau, L. M.; Wilkinson, E. C.; Que, L., Jr; Tolman, W. B. *J. Am. Chem. Soc.* **1997**, *119*, 8217−8227.
(23) Magnuson, A.; Berglund, H.; Korall, P.; Hammarström, L.; Akermark, B.; Styring, S.; Sun, L. *J. Am. Chem. Soc.* **1997**, *119*, 10720−10725.
(24) Jonker, G. H.; Van Santen, J. H. *Physica* **1950**, *16*, 337
(25) Anderson, P. W.; Hasegawa, H. *Phys. Rev.* **1955**, *100*, 675−681.
(26) Rao, C. N. R.; Cheetham, A. K. *Science* **1997**, *276*, 911−912 and references therein.
(27) Kipke, C. A.; Scott, M. J.; Gohdes, J. W.; Armstrong, W. H. *Inorg. Chem.* **1990**, *29*, 2193-2194.
(28) Ziolo, R. F.; Stanford R. H.; Rossman, G. R.; Gray, H. B. *J. Am. Chem. Soc.* **1974**, *96*, 7910−7915.
(29) Vogt, L. H.; Zalkin, A.; Templeton, D. H. *Inorg. Chem.* **1967**, *6*, 1725−1730.
(30) Kitajima, N.; Osawa, M.; Tanaka, M.; Moro-oka, Y. *J. Am. Chem. Soc.* **1991**, *113*, 8952−8953.
(31) Schardt, B. C.; Hollander, F. J.; Hill, C. L. *J. Am. Chem. Soc.* **1982**, *104*, 3964−3972.
(32) Gruenwedel, D. W. *Inorg. Chem.* **1968**, *7*, 495−501.

and ethyl acetate (2:1). Acetonitrile was distilled over CaH_2 and under argon before use.

***N,N*-Bis(2-pyridylmethyl)-*N′*-(2-hydroxybenzyl)ethane-1,2-diamine.** This ligand was obtained by the following two-step synthesis:

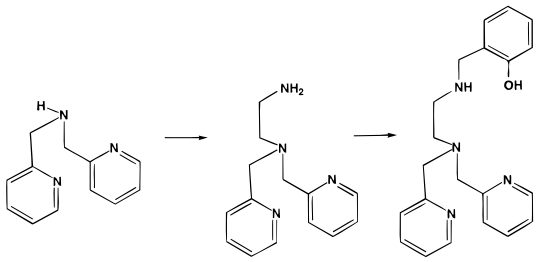

The details of the synthesis are described below.

Step 1: *N,N*-Bis(2-pyridylmethyl)ethane-1,2-diamine. A mixture of 5.14 g (25.8 mmol) *N,N*-bis(2-pyridylmethyl)-amine, 6.56 g (25.8 mmol) of *N*-(2-bromoethyl)-phthalimide, 8 g of anhydrous K_2CO_3, and 0.43 g (2.58 mmol) of KI in 75 mL of CH_3CN was allowed to reflux overnight. After cooling and concentrating under vacuum, the remaining brown oil was chromatographed on basic aluminum oxide (activity II−III) with CH_2Cl_2 as eluant. After removal of the first fraction, which contained the residual *N*-(2-bromoethyl)-phthalimide, concentration of the second fraction led to the precipitation of an orange solid. This solid was dissolved in 65 mL of absolute ethanol containing 0.78 mL (25.8 mmol) of $N_2H_4 \cdot H_2O$. The mixture was allowed to reflux for 3 h. After cooling, 21.5 mL of 12 N HCl (258 mmol) was added, and the mixture was stirred for another hour. The solution was then filtered to remove the white precipitate, and ethanol was removed under vacuum. To this aqueous mixture was added an aqueous NaOH solution. The aqueous phase was extracted three times with CH_2Cl_2. The combined CH_2Cl_2 extracts were dried over Na_2SO_4, filtered, and then concentrated under vacuum. Brown oil (3.293 g) was obtained (53% yield). ^{1}H NMR (200 MHz,$CDCl_3$): δ 8.42−8.40 (m, 2H, C_5H_4N), 7.57−7.00 (m, 6H, C_5H_4N), 3.73 (s, 4H, CH_2), 2.61 (dt, 4H, $J = 27.95$ Hz, $J = 5.60$ Hz, CH_2CH_2), 1.32 (m, 2H, NH_2). ^{13}C NMR (62.9 MHz, $CDCl_3$): δ 158.4, 147.8, 135.2, 121.8, 120.8, 59.4, 56.1, 38.4. MS CI/NH_4^+: 243 (M + 1).

Step 2: *N,N*-Bis(2-pyridylmethyl)-*N′*-(2-hydroxybenzyl)ethane-1,2-diamine. In 18 mL of absolute ethanol, 0.511 g (2.11 mmol) of *N,N*-bis(2-pyridylmethyl)ethane-1,2-diamine and 0.22 mL (2.11 mmol) of salicylaldehyde were dissolved with 0.133 g (2.11 mmol) of $NaBH_3CN$ and 0.32 mL (4.22 mmol) of trifluoroacetic acid. The solution was stirred overnight and an aqueous NaOH (15%) solution was added. The mixture was then concentrated to evaporate ethanol and extracted three times with CH_2Cl_2. The combined extracts were dried over Na_2SO_4, filtered, and then concentrated under vacuum. A yellow oil (0.702 g) was obtained (96% yield), characterized as *N,N*-bis(2-pyridylmethyl)-*N′*-(2-hydroxybenzyl)ethane-1,2-diamine. ^{1}H NMR (200 MHz, $CDCl_3$): δ 8.51−8.49 (m, 2H, C_5H_4N), 7.62−7.01 (m, 6H, C_5H_4N), 6.89−6.58 (m, 4H, C_6H_4OH), 3.74 (s, 4H, CH_2), 3.66 (s, 2H, CH_2), 2.64 (br s, 4H, CH_2CH_2). ^{13}C NMR (62.9 MHz,$CDCl_3$): δ 159.3, 158.3, 148.9, 136.1, 128.5, 128.0, 123.7, 122.6, 121.7, 116.7, 116.2, 60.0, 52.9, 51.3, 45.4. MS CI/NH_4^+: 349 (M + 1).

***N,N*-Bis(2-pyridylmethyl)-*N′*-(2-hydroxybenzyl-*d*$_4$)ethane-1,2-diamine.** The ligand deuterated on the phenol ring was prepared using totally deuterated salicylaldehyde which was synthesized from d_6-phenol (99 atom % D, Aldrich) by adapting the phenol formylation process reported in ref 33. The reaction was carried out in D_2O under argon, with use of $CDCl_3$ instead of $CHCl_3$. The mixture was extracted three times with CH_2Cl_2. The combined extracts were dried over Na_2SO_4, filtered, and then concentrated under vacuum. The remaining yellow oil was chromatographed on basic aluminum oxide (activity II−III) with CH_2Cl_2 as eluant. Concentration of the first fraction gave totally deuterated salicylaldehyde. Deuteration was checked by ^{1}H and ^{2}H NMR.

(33) Furniss, B. S.; Hannaford, A. J.; Rogers, V.; Smith, P. W. G.; Tatchell, A. R. *Vogel's Textbook of Practical Organic Chemistry*; Longman: London, 1978.

$[Mn^{III}_2O(N,N$-bis(2-pyridylmethyl)-$N′$-salicylidene-ethane-1,2-diamine)$_2](ClO_4)_2 \cdot$EtOH. To a solution of 0.528 g (1.52 mmol) of *N,N*-bis(2-pyridylmethyl)-*N′*-(2-hydroxybenzyl)ethane-1,2-diamine in 7 mL of absolute ethanol was added 0.407 g (1.52 mmol) of $Mn(O_2CCH_3)_3 \cdot 2H_2O$. The resulting brown solution was filtered, and to the filtrate was added a EtOH solution (5 mL) of $NaClO_4 \cdot H_2O$ (0.426 g, 3.04 mmol). A brown microcrystalline solid precipitated immediately. The mixture was stirred for an additional 1/4 h. The solid was collected by filtration, washed thoroughly with absolute ethanol, and dried under vacuum. This procedure afforded 200 mg of $(C_{42}H_{42}Mn_2N_8O_3)(ClO_4)_2 \cdot$EtOH (25% yield with respect to manganese). Anal. Calcd for $(C_{42}H_{42}Mn_2N_8O_3)(ClO_4)_2 \cdot$EtOH: Mn, 10.37; C, 49.76; H, 4.52; N, 10.56; Cl, 9.87. Found Mn, 10.37; C, 49.76; H, 4.87; N, 10.67; Cl, 9.08. Significant IR bands (cm^{-1}): 3440 (br), 1627 (s), 1601 (s), 1478 (s), 1445 (s), 1297 (m), 1270 (s), 1094 (vs), 1016(w), 857 (s), 800 (m), 763 (s), 622 (s). Symbols: br, broad; vs, very strong; s, strong; m, medium; w, weak; sh, shoulder. Single crystals were grown by slow diffusion of a mixture of $CH_2Cl_2/CHCl_3$ (1:1), in a concentrated solution in CH_3CN. X-ray diffraction (see Discussion) showed that the formation of this complex was accompanied by the spontaneous dehydrogenation of the (*N,N*-bis(2-pyridylmethyl)-*N′*-(2-hydroxybenzyl)ethane-1,2-diamine) ligand leading to the formation of the Schiff base with the hydroxybenzyl group. The analysis found by X-ray diffraction was different from the powder described above and led to the following formula: $(C_{42}H_{42}Mn_2N_8O_3)(ClO_4)_2 \cdot 2.23CHCl_3 \cdot 0.65CH_2Cl_2$. The powder and the crystalline samples will be referred to as $[Mn_2OL_2](ClO_4)_2 \cdot$EtOH and **$[Mn_2OL_2](ClO_4)_2$**, respectively, in the text.

$[Mn^{III}Mn^{IV}O(N,N$-bis(2-pyridylmethyl)-$N′$-salicylidene-ethane-1,2-diamine)$_2)](ClO_4)_{2.37}(PF_6)_{0.63} \cdot 1.5CH_3CN$. Preparative scale electrolysis of a 10^{-2} M solution of $[Mn_2OL_2](ClO_4)_2 \cdot$EtOH in CH_3CN containing 0.1 M tetraethylammonium perchlorate was performed. The potential was set to 0.84 V/saturated calomel electrode (SCE). The total number of Coulombs required to complete the electrolysis corresponded to a one-electron oxidation per mole of the starting complex. After a few days at −12 °C, 30 mg of a fine powder (53% yield) was collected from the resulting oxidized solution. Because of the small quantity obtained, chemical analysis of the powder was not pursued. Significant IR bands (cm^{-1}): 3422 (br), 1620 (s), 1601 (s), 1541(m), 1482 (m), 1443 (s), 1295 (s), 1257 (m), 1090 (vs), 1034 (w), 1017 (w), 910(w), 857 (s), 805 (m), 763 (s), 623 (s). Single crystals were obtained by slow diffusion of Et_2O in a concentrated CH_3CN solution of the powder collected from the electrolysis. X-ray diffraction revealed the composition $(C_{42}H_{42}Mn_2N_8O_3)(ClO_4)_{2.37}(PF_6)_{0.63} \cdot 1.5CH_3CN$. The PF_6^- was introduced inadvertently by using a contaminated electrolyte. This compound will be referred to as **$[Mn_2OL_2](ClO_4)_{2.37}(PF_6)_{0.63}$** in the text. These crystals were used for X-ray diffraction and magnetic susceptibility measurements. The analogue compound with perchlorate counteranions only was prepared. Crystals of poorer quality were obtained which led to a similar structure and the following formula: $(C_{42}H_{42}Mn_2N_8O_3)(ClO_4)_3 \cdot CH_3CN \cdot H_2O$. EPR, Raman, and UV−vis experiments were made on electrochemically prepared solutions.

Magnetic Susceptibility Measurements. Magnetic susceptibility measurements in the 4.2−300 K temperature range were carried out with a MPMS5 SQUID susceptometer (Quantum Design Inc.). The calibration was made at 298 K using a palladium reference sample furnished by Quantum Design Inc. Ground crystals of **$[Mn_2OL_2](ClO_4)_2$** and **$[Mn_2OL_2](ClO_4)_{2.37}(PF_6)_{0.63}$** were used.

Crystallographic Data Collection and Refinement of the Structures of $[Mn_2OL_2](ClO_4)_2$ and $[Mn_2OL_2](ClO_4)_{2.37}(PF_6)_{0.63}$. The crystal data of **$[Mn_2OL_2](ClO_4)_2$** and **$[Mn_2OL_2](ClO_4)_{2.37}(PF_6)_{0.63}$** and the parameters of data collections are summarized in Table 1. A hexagonal prismatic brownish black crystal of **$[Mn_2OL_2](ClO_4)_2$** with the dimensions 0.8 × 0.7 × 0.7 mm and a dark brown crystal of **$[Mn_2OL_2](ClO_4)_{2.37}(PF_6)_{0.63}$** with a prismatic shape with the dimensions 0.5 × 0.35 × 0.2 mm were chosen for X-ray diffraction experiments. The unit-cell and intensity data were measured with an Enraf-Nonius CAD-4 diffractometer with graphite monochromated Mo Kα radiation ($\lambda = 0.71073$ Å). The cell constants were refined by least-squares procedures based on the 2Θ values of 25 reflections measured in the ranges $20.06 < 2\Theta < 21.85°$ for **$[Mn_2OL_2](ClO_4)_2$** and $23.7 < 2\Theta < 32.16°$ for **$[Mn_2OL_2](ClO_4)_{2.37}(PF_6)_{0.63}$** at ambient temperature. All

Table 1. Crystallographic Data for **$[Mn_2OL_2](ClO_4)_2$** and **$[Mn_2OL_2](ClO_4)_{2.37}(PF_6)_{0.63}$**

	$[Mn_2OL_2](ClO_4)_2$	$[Mn_2OL_2](ClO_4)_{2.37}(PF_6)_{0.6}$
formula	$[C_{42}H_{42}Mn_2N_8O_3]_2[ClO_4]$ 2.23$[CHCl_3]$ 0.65$[CH_2Cl_2]$	$[C_{42}H_{42}Mn_2N_8O_3]$ {2.38$[ClO_4]$ 0.62$[PF_6]$} 1.5 $[CH_3CN]$
fw	1337.05	1204.88
temp, K	294	294
radiation	Mo Kα (0.710 73 Å)	Mo Kα (0.710 73 Å)
space group	$P\bar{1}$	$P2_1/n$
a, Å	12.463(9)	12.067(2)
b, Å	12.78(2)	21.241(5)
c, Å	21.55(1)	20.357(3)
α, deg	73.20(6)	90
β, deg	86.37(5)	103.87(1)
γ, deg	61.02(6)	90
V, Å^3	2863(5)	5066(2)
Z	2	4
D_x, g/cm^3	1.547	1.583
μ, mm^{-1}	0.969	0.730
N_{total}	9651	9148
N_{indep}	9379	8888
R	0.073	0.047
R_w	0.200	0.121
$\Delta\rho_{max}$ (e Å^{-3})	0.553	0.584
$\Delta\rho_{min}$ (e Å^{-3})	−0.697	−0.417

reflection intensities were collected in the range $4 < 2\Theta < 50°$ within $[-14 < h < 14, -14 < k < 15, 0 < l < 25]$ for **$[Mn_2OL_2](ClO_4)_2$** and $[-14 < h < 13, 0 < k < 25, 0 < l < 24]$ for **$[Mn_2OL_2](ClO_4)_{2.37}(PF_6)_{0.63}$**. The total numbers of the collected independent reflections are 9379 for **$[Mn_2OL_2](ClO_4)_2$** and 8888 for **$[Mn_2OL_2](ClO_4)_{2.37}(PF_6)_{0.63}$**. Both structures were solved by direct methods with the program SHELXS86[34] and refined by using the SHELXL93[35] program. The drawings were prepared with ORTEPII.[36]

$[Mn_2OL_2](ClO_4)_2$. Two crystallographically independent molecules A and B in the unit cell were identified. In both, the bridging oxygen atom is positioned on different centers of symmetry (0, 0, 0 and 0, 0, 0.5). Particular disorder is observed in molecule B (the C26 atom occupies two positions with identical populations). Two perchlorate anions and all molecules of solvent (trichloro- and dichloromethane molecules) are disordered.

$[Mn_2OL_2](ClO_4)_{2.37}(PF_6)_{0.63}$. The structure of this complex consists of a linear molecular cation, disordered anions, and solvent molecules. One ClO_4^- is distributed over two sites with nonidentical occupations (0.85 and 0.15). A second anion is a superposition of ClO_4^- (site occupation factor of 0.75) and PF_6^- but with a smaller occupation factor (0.25). A third anion site shows also a superposition of ClO_4^- (site occupation factor of 0.62) and PF_6^- (0.38). In addition, two molecules of acetonitrile were identified, one of them in a general position and the second one distributed over two positions at the inversion center.

Both structures were refined by full-matrix least-squares approximation based on F^2. Refinement was anisotropic for non-H atoms of cations, isotropic for disordered anions and solvent molecules. Hydrogen positions were calculated by assuming geometrical positions and were included in the structural model. Final refinement of this model was continued until convergence when R1 = 0.073 for $F^2 > 2\sigma(F2)$ and RW = 0.200 for **$[Mn_2OL_2](ClO_4)_2$** and R1 = 0.047 for $F^2 > 2\sigma(F2)$ and RW = 0.121 for **$[Mn_2OL_2](ClO_4)_{2.37}(PF_6)_{0.63}$**. The final difference map showed the largest residual peaks of 0.55 and −0.69 e Å^{-3} in **$[Mn_2OL_2](ClO_4)_2$** and 0.58 and −0.41 e Å^{-3} in **$[Mn_2OL_2](ClO_4)_{2.37}(PF_6)_{0.63}$**.

Atomic coordinates for all atoms, bond distances and angles, and thermal parameters have been deposited at the Cambridge Crystallographic Data Centre (CCDC) and can be obtained on request at CCDC, Union Road, Cambridge C82 IEZ, UK.

Cyclic Voltammetry and Preparative Scale Electrolysis. Cyclic voltammetry and controlled potential electrolysis were measured using an EGG PAR potentiostat (M273 model). For cyclic voltammetry, the working electrode was a platinum disk of 3-mm diameter, carefully polished with diamond pastes and ultrasonically rinsed in ethanol before use. Preparative scale electrolyses were carried out using a cylindrical Pt grid of 20-mm diameter and 50-mm height serving as the working electrode in a cylindrical cell filled with 20 mL of solution. A Pt wire was used as the counter electrode and a $Ag/AgClO_4$ electrode prepared in acetonitrile, separated by a fritted disk from the main solution as the reference electrode (270 mV above the potential of the saturated calomel electrode). For preparative scale electrolysis experiments, the counter electrode was separated from the cathodic compartment by a fritted bridge. The experiments were carried out in carefully degassed solutions by argon flushing.

UV−Vis Spectroelectrochemistry. The thin-layer cell used for room-temperature UV−vis experiments was described previously.[37] The working electrode was a platinum grid (0.3 mm). Reference and counter electrodes were the same as used for cyclic voltammetry. Optical path of the cell was 0.5 mm. The spectra were obtained on a UV−Vis Varian Cary 5E spectrophotometer.

EPR Spectroscopy. EPR spectra were recorded on Bruker ESP 300 E spectrometer. For low-temperature studies, an Oxford Instruments continuous flow helium cryostat and a temperature control system were used.

EPR Simulation. Simulation of the EPR spectrum was performed using a FORTRAN program for powder spectra of $S = {}^1/_2$ systems, including calculation of the hyperfine contributions to the second order.[38] For each transition, the resonant field was calculated using perturbation theory up to the second order for the hyperfine coupling terms and the resulting stick spectrum was then convoluted with Gaussian functions. This simulation program is coupled to a minimization program to find the set of parameters giving the lowest possible value of the agreement factor defined as $R = \sum_i(Y_i^{calc} - Y_i^{exp})^2/\sum_i(Y_i^{exp})^2$.

Resonance Raman Spectroscopy. Resonance Raman spectra were recorded using a Jobin-Yvon U1000 double monochromator equipped with a liquid-nitrogen−cooled, charge-coupled device (CCD) detector. Light excitation at 413.1 nm was provided by a Kr^+ laser (Coherent Innova 90); less than 15 mW of laser power at the sample was used. The spectra were the result of the average of at least 10 exposures of 250 s each. The samples (ca. 5×10^{-4} M) in acetonitrile were held in a cold gas-flow cryostat (TBT, France) at 15 K. Spectra were calibrated at the 920 cm^{-1} band of acetonitrile.

Results

Structure of $[Mn_2OL_2](ClO_4)_2$. The unit cell contains two independent molecules A and B. Distances and angles pertaining to the inner coordination of Mn are listed in Table 2. The structures of these molecules are very similar, and only one type of dication $[Mn_2OL_2]^{2+}$ is represented in Figure 1 (1) and discussed below. It contains a linear Mn−O−Mn unit, the oxygen atom being on an inversion center. The Mn(III)−O_{oxo} distance [1.758(2) Å] must be compared with the corresponding distances in the Mn(III)−O−Mn(III) core of $Mn_2O(5\text{-}NO_2\text{-saldien})_2$[27] [1.751(4) Å, 1.757(4) Å], $Mn_2OL'_2$ [L′ stands for the oxygenation product of $HB(3,5\text{-}{}^iPr_2pz)_3$, 1.77(1) Å],[30] and in the tetranuclear manganese complex $\{[Mn_2(tphpn)(O_2CCH_3)(H_2O)]_2O\}^{4+}$ [39] [1.766(1) Å]. These distances are slightly shorter than the corresponding ones observed in the complexes containing the μ-oxo-bis(μ-acetato) core such as $[Mn_2O(O_2CCH_3)_2$-

(34) Sheldrick, G. M. *SHELXS86: Program for the solution of crystal structures*; University of Göttingen: Germany, 1986.
(35) Sheldrick, G. M. *SHELXL93: Program for the refinement of crystal structures*; University of Göttingen: Germany, 1993.
(36) Johnson, C. K. *ORTEPII*; Report ORNL-5138; Oak Ridge National Laboratory: Oak Ridge, TN, 1976.
(37) Frapart, Y.-M.; Boussac, A.; Albach, R.; Anxolabéhère-Mallart, E.; Delroisse, M.; Verlhac, J. B.; Blondin, G.; Girerd, J.-J.; Guilhem, J.; Césario, M.; Rutherford, A. W.; Lexa, D. *J. Am. Chem. Soc.* **1996**, *118*, 2669−2678.
(38) Bonvoisin, J.; Blondin, G.; Girerd, J.-J.; Zimmermann, J.-L. *Biophys. J.* **1992**, *61*, 1076−1086.
(39) Chan, M. K.; Armstrong, W. H. *J. Am. Chem. Soc.* **1989**, *111*, 9121−9122.

Table 2. Selected Bond Lengths [Å] and Angles [deg] for $[Mn_2OL_2](ClO_4)_2$ and $[Mn_2OL_2](ClO_4)_{2.37}(PF_6)_{0.63}$

$[Mn_2OL_2](ClO_4)_2$[a]		$[Mn_2OL_2](ClO_4)_{2.37}(PF_6)_{0.63}$		
			Mn(IV)	Mn(III)
Mn−O	1.758(2)	Mn−O	1.727(2)	1.797(2)
Mn−O(1)	1.924(4)	Mn−O(1)	1.853(3)	1.887(3)
Mn−N(17)	2.168(5)	Mn−N(2)	2.046(3)	2.143(3)
Mn−N(10)	2.226(6)	Mn−N(3)	2.007(3)	2.251(4)
Mn−N(24)	2.248(6)	Mn−N(4)	2.004(4)	2.236(4)
Mn−N(9)	2.000(5)	Mn−N(1)	1.997(3)	1.989(3)
			Mn(IV)	Mn(III)
O−Mn−O(1)	95.40(14)	O−Mn−O(1)	93.07(12)	92.31(12)
O−Mn−N(9)	174.9(2)	O−Mn−N(1)	176.15(14)	175.9(2)
O(1)−Mn−N(9)	89.3(2)	O(1)−Mn−N(1)	89.98(13)	90.32(13)
O−Mn−N(17)	92.8(2)	O−Mn−N(4)	90.92(13)	90.79(13)
O(1)−Mn−N(17)	169.9(2)	O(1)−Mn−N(4)	99.21(14)	105.95(14)
N(9)−Mn−N(17)	82.8(2)	N(1)−Mn−N(4)	86.3(2)	85.5(2)
O−Mn−N(10)	91.7(2)	O−Mn−N(3)	89.51(13)	88.21(12)
O(1)−Mn−N(10)	108.4(2)	O(1)−Mn−N(3)	98.14(13)	101.54(14)
N(9)−Mn−N(10)	84.9(2)	N(1)−Mn−N(3)	92.4(2)	94.3(2)
N(17)−Mn−N(10)	77.3(2)	N(4)−Mn−N(3)	162.60(14)	152.51(13)
O−Mn−N(24)	89.6(2)	O−Mn−N(2)	93.58(13)	95.01(12)
O(1)−Mn−N(24)	99.3(2)	O(1)−Mn−N(2)	173.30(12)	172.04(13)
N(9)−Mn−N(24)	91.6(2)	N(1)−Mn−N(2)	83.42(14)	82.54(14)
N(17)−Mn−N(24)	74.7(2)	N(4)−Mn−N(2)	81.54(14)	77.12(13)
N(10)−Mn−N(24)	152.0(2)	N(3)−Mn−N(2)	81.07(14)	75.61(13)
Mn(#)−O−Mn	180	MnA−O−MnB	178.7(2)	

[a] $[Mn_2OL_2](ClO_4)_2$ symmetry transformations used to generate equivalent atoms: # [−*x*, −*y*, −*z*] for molecule A and # [−*x*, −*y*, −*z* + 1] for molecule B.

$(TACN)_2]^{2+}$ [40] [1.80(1) Å] or $[Mn_2O(O_2CCH_3)_2(bpy)_2(H_2O)_2]^{2+}$ [41] 41 [1.777(12) Å, 1.788(11) Å]. In $[Mn_2O(CN)_{10}]^{6-}$ [1.723(4) Å][28] and $Mn_2O(phthal)_2(py)_2$[29] [1.71(1) Å], the Mn−O distances are shorter than all the previous ones, an effect likely caused by a low-spin state for the Mn(III) ions. Although in the $Mn_2O(5\text{-}NO_2saldien)_2$ complex the Mn−O−Mn unit is nonlinear (168.4°), we observe for $[Mn_2OL_2]^{2+}$ a linear Mn(III)−O−Mn(III) bridge. The distance between the phenoxy oxygen atom and manganese in $[Mn_2OL_2]^{2+}$ [Mn−O1 = 1.924(4) Å] is similar to the corresponding one observed in the complex $Mn_2O(5\text{-}NO_2saldien)_2$ [1.917(4) Å]. In $[Mn_2OL_2]^{2+}$ the Mn−N17(amine) is 2.168(5) Å. The Mn−N24(py) = 2.248(6) Å and Mn−N10(py) = 2.226(6) Å distances lying perpendicular to the Mn−O−Mn axis are the two longest around each Mn(III), which suggests that the Mn(III) ions exhibit a Jahn−Teller elongation along the N24−N10 axis. This is confirmed by the MO calculation (see below) which shows that the fourth unpaired electron on Mn(III) is in a MO containing a large percentage of d_{z^2} orbital, the *z* axis corresponding to the N24−N10 axis. A Mn(III) monomer with a related hexadentate ligand, *N*,*N*-bis(2-pyridylmethyl)-*N*′,*N*′-bis(2-hydroxybenzyl)-1,2-diaminoethane, has been structurally characterized.[42] The Jahn−Teller elongation axis is similarly along the N_{py}−Mn−N_{py} axis [Mn−N_{py} 2.252(5) Å, 2.237(5) Å].

The observation of a short N9−C8 distance [1.277(8) Å] indicated the dehydrogenation of the ligand during the complex synthesis as follows

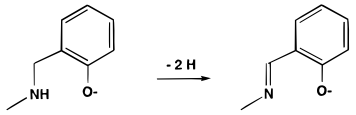

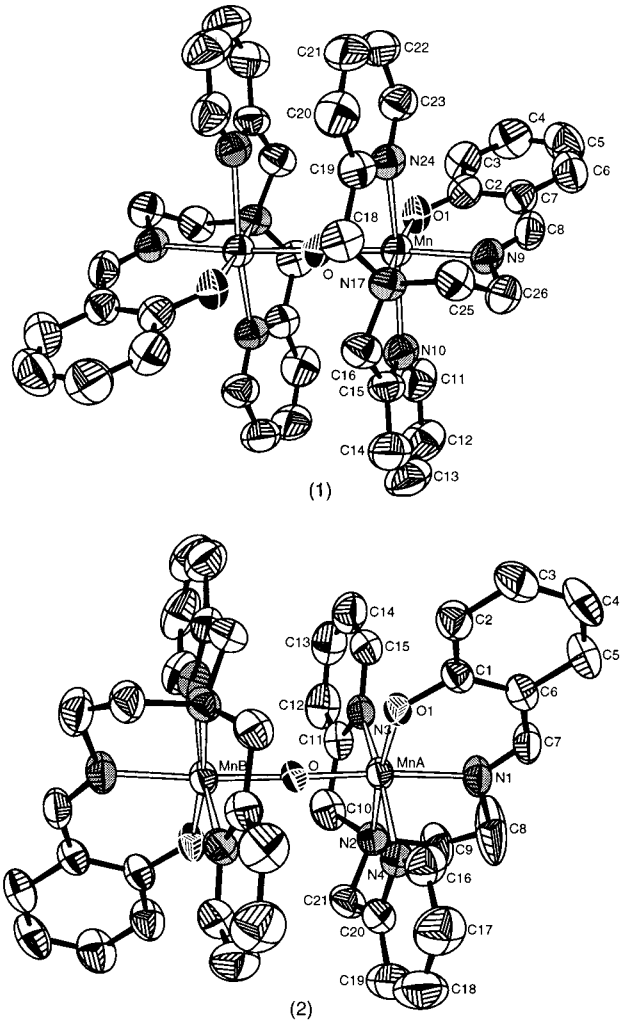

Figure 1. ORTEP diagram of $[Mn_2OL_2]^{2+}$ (1) and $[Mn_2OL_2]^{3+}$ (2) with thermal ellipsoids at 50% probability. For $[Mn_2OL_2]^{2+}$ only one crystallographically independent molecule is shown.

This behavior has already been reported for Co monomeric complexes.[43] In $[Mn_2OL_2]^{2+}$, the Mn−N9(imine) is 2.000(5) Å.

Structure of $[Mn_2OL_2](ClO_4)_{2.37}(PF_6)_{0.63}$. The structure of the $[Mn_2OL_2]^{3+}$ cation is shown in Figure 1 (2). As may be observed, the linear Mn−O−Mn core is preserved. Selected distances and angles pertaining to the inner coordination of Mn are listed in Table 2. The inequivalence between the Mn(IV) (Mn_A) and the Mn(III) (Mn_B) is observable from the bond distances. The Mn_A-O_{oxo} distance of 1.727(2) Å is, as expected, shorter than the Mn_B-O_{oxo} distance of 1.797(2) Å. The Mn(IV)−O_{oxo} distance is shorter than in $[N_3Mn^{IV}(TPP)]_2O$ [1.794(4) Å, 1.743(4) Å].[31] Upon oxidation of $[Mn_2OL_2]^{2+}$, the O_{oxo} moves closer to the Mn(IV) atom, the Mn−Mn distance remaining almost constant (3.516 Å in $[Mn_2OL_2]^{2+}$ and 3.524 Å in $[Mn_2OL_2]^{3+}$). The Mn(III) coordination sphere is slightly different from those observed in $[Mn_2OL_2]^{2+}$. The Mn_B-O_{oxo} distance is longer than those in $[Mn_2OL_2]^{2+}$. The Mn_B−O1, Mn_B−N2(amine), and Mn_B−N1(imine) distances are shorter than the corresponding ones in $[Mn_2OL_2]^{2+}$ because of the

(40) Wieghardt, K.; Bossek, V.; Ventur, D. J.; Weiss, J. *J. Chem. Soc., Chem. Commun.* **1985**, 347−349.
(41) Ménage, S.; Girerd, J.-J.; Gleizes, A. *J. Chem. Soc., Chem. Commun.* **1988**, 431−432.
(42) Neves, A.; Erthal, S. M. D.; Vencato, I.; Ceccato, A. S.; Mascarambas, Y. P.; Nascimento, O. R.; Hörner, M.; Batista, A. A. *Inorg. Chem.* **1992**, *31*, 4749−4755.
(43) Böttcher, A.; Elias, H.; Jäger, E. G.; Langfelderova, H.; Mazur, M.; Müller, L.; Paulus, H.; Pelikan, P.; Rudolph, M.; Valko, M. *Inorg. Chem.* **1993**, *32*, 4131−4138.

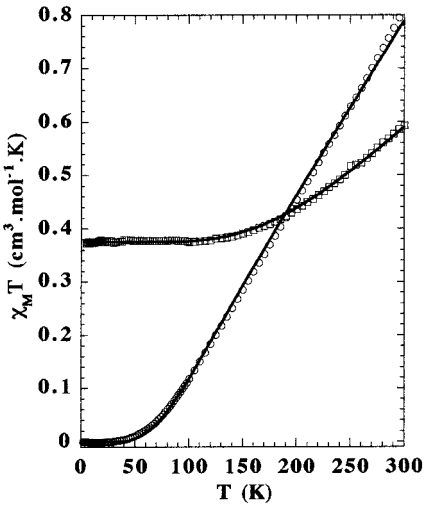

Figure 2. Product of the magnetic susceptibility per mole by temperature for **[Mn$_2$OL$_2$](ClO$_4$)$_2$** (○) and **[Mn$_2$OL$_2$](ClO$_4$)$_{2.37}$(PF$_6$)$_{0.63}$** (□). Solid lines were generated by the best-fit parameter given in the text.

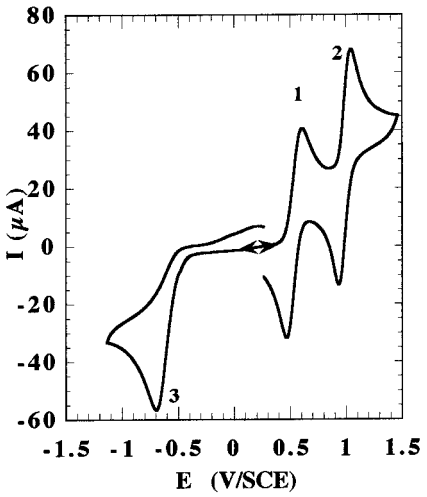

Figure 3. Cyclic voltammetry of [Mn$_2$OL$_2$]$^{2+}$ in acetonitrile, with 0.1 M TBAClO$_4$ as the supporting electrolyte. Potentials are referenced vs SCE.

decrease of electron density on Mn(III), which itself is a consequence of the slight off-shift of the oxo group. The Mn$_B$−N3(py) and Mn$_B$−N4(py) distances are similar to those in [Mn$_2$OL$_2$]$^{2+}$: 2.251(4) and 2.236(4) Å. Around the Mn(IV) ion, the Mn−O(phenoxy) is shorter than for the Mn(III) by 0.04 Å. The Mn$_A$−N2(amine) is 2.046(3) Å and the Mn$_A$−N3(py) and Mn$_A$−N4(py) are 2.007(3) Å and 2.004(4) Å, respectively; these three distances are shorter than the corresponding Mn(III)−N bond lengths. The most dramatic change upon oxidation is the shortening of ≈0.24 Å of the Mn−N(pyridine) bonds. This is in agreement with the proposal that the Mn-py axis defines the Jahn−Teller elongation for the Mn(III). The Mn$_A$−N1(imine) bond *trans* to the oxo group is 1.997(3) Å; it tends to be slightly larger than the analogous Mn$_B$−N1(imine) = 1.989(3) Å. This could be related to the increase of *trans* effect when the oxo group is brought close to the Mn$_A$ atom. To our knowledge, this is the first structurally characterized complex with a linear Mn(III)−O−Mn(IV) unit. Such a species has been proposed from EPR data with TPP^{2-} as a ligand but has not been isolated.[44,45]

Magnetic Susceptibility. For both compounds, **[Mn$_2$OL$_2$](ClO$_4$)$_2$** and **[Mn$_2$OL$_2$](ClO$_4$)$_{2.37}$(PF$_6$)$_{0.63}$**, the molar magnetic susceptibility χ_M was measured on ground crystals as a function of the temperature T. The results for **[Mn$_2$OL$_2$](ClO$_4$)$_2$** are shown in Figure 2 in the form of the $\chi_M T$ versus T plot, together with the results obtained for **[Mn$_2$OL$_2$](ClO$_4$)$_{2.37}$(PF$_6$)$_{0.63}$**.[46] The $\chi_M T$ value for **[Mn$_2$OL$_2$](ClO$_4$)$_2$** decreases from 0.812 cm^3 mol^{-1} K at 300 K to 0 cm^3 mol^{-1} K for $T \leq 50$ K. This behavior is characteristic of a strong antiferromagnetic coupling between the two $S = 2$ spins of high-spin Mn(III) ions. The $\chi_M T$ value was calculated according to

$$\chi_M T = (N\beta^2 g^2/3k)(\Sigma S(S+1)(2S+1)) \times \exp(J(S(S+1)/2kT))/\Sigma(2S+1)\exp(J(S(S+1)/2kT))$$

where J is the exchange constant in the Heisenberg Hamiltonian $H = -J\mathbf{S_1}\cdot\mathbf{S_2}$. The best fit was obtained with $g = 2$ (kept constant) and $J = -216$ cm^{-1}. The magnitude and sign of the J value are comparable with those found by Kipke et al.[27] for a similar linear Mn(III)−O−Mn(III) core ($J = -240$ cm^{-1}).

The $\chi_M T$ value for **[Mn$_2$OL$_2$](ClO$_4$)$_{2.37}$(PF$_6$)$_{0.63}$** decreases from 0.59 cm^3 mol^{-1} K at 300 K to a plateau at 0.35 cm^3 mol^{-1} K beginning around 115 K. This is characteristic of an antiferromagnetic coupling between the electronic spins of the high-spin Mn(IV) ($S = {}^3/_2$) and Mn(III) ($S = 2$) ions which produces a spin $S = {}^1/_2$ ground state. The experimental results were simulated using the same expression as the one used for compound **[Mn$_2$OL$_2$](ClO$_4$)$_2$**. The best fit was obtained by setting $g = 2$ for $J = -353$ cm^{-1}.

In summary these measurements are in full agreement with the oxidation states deduced from the structural study. The [Mn$_2$OL$_2$]$^{2+}$ complex contains a pair of Mn(III) ions antiferromagnetically coupled to give an electronic spin singlet ground state and the [Mn$_2$OL$_2$]$^{3+}$ complex contains a Mn(III)Mn(IV) pair in which antiferromagnetic coupling leads to an electronic spin doublet ground state.

Redox Properties of [Mn$_2$OL$_2$]$^{2+}$. Cyclic voltammetry of [Mn$_2$OL$_2$]$^{2+}$ in acetonitrile (Figure 3) shows two reversible anodic waves at $E_1{}^{1/2} = 0.54$ V/SCE (wave 1), and $E_2{}^{1/2} = 0.99$ V/SCE (wave 2). In reduction one irreversible cathodic wave observed at $E_p = -0.69$ V/SCE indicates that the Mn(III)Mn(II) mixed-valent species is unstable under these conditions. In oxidation, controlled potential electrolysis at +0.84 V/SCE established a one-electron (for two Mn) oxidation process leading to the formation of the mixed-valence Mn(III)Mn(IV) compound. Preparative scale electrolysis was performed at +0.84 V/SCE on a concentrated solution of [Mn$_2$OL$_2$]$^{2+}$ (5 mM), and a dark fine powder was obtained, from which crystals were grown leading to the identification of the complex as the [Mn$_2$OL$_2$]$^{3+}$ form. The presence of the second reversible anodic wave indicates that a species with higher oxidation level is accessible (see below). As expected from the electron donor properties of the phenolic ligand, these potentials are lower than those reported in Mn(III)μ-oxo-bis(μ-acetato)Mn(III) complexes with the same total charge. For example in acetonitrile, $E^{1/2}$ is reported at +0.89 V/SCE for the Mn(III)Mn(IV)/Mn(III)Mn(III) couple of [Mn$_2$O(O$_2$CCH$_3$)$_2$(*N*,*N*′,*N*″-trimethyl-TACN)$_2$]$^{2+}$.[47]

(44) Camenzind, M. J.; Schardt, B. C.; Hill, C. L. *Inorg. Chem.* **1984**, *23*, 1984−1986.
(45) Dismukes, G. C.; Sheats, J. E.; Smegal, J. A. *J. Am. Chem. Soc.* **1987**, *109*, 7202−7203.
(46) The data shown in Figure 2 for **[Mn$_2$OL$_2$](ClO$_4$)$_2$** have been corrected for 0.41% of a S = $^5/_2$ Mn(II) impurity and those for **[Mn$_2$OL$_2$](ClO$_4$)$_{2.38}$(PF6)$_{0.62}$** for 0.8% of a S = $^5/_2$ Mn(II) impurity.
(47) Wieghardt, K.; Bossek, U.; Nuber, B.; Weiss, J.; Bonvoisin, J.; Corbella, M.; Vitols, S. E.; Girerd, J.-J. *J. Am. Chem. Soc.* **1988**, *110*, 7398−7411.

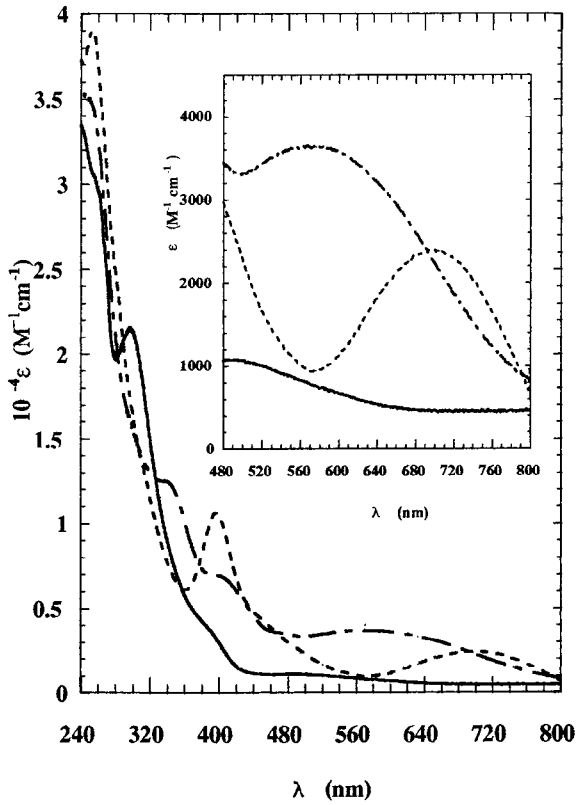

Figure 4. Spectroelectrochemistry of $[Mn_2OL_2]^{2+}$ in acetonitrile with 0.1 M $TBAClO_4$ as supporting electrolyte. Spectrum of $[Mn_2OL_2]^{2+}$ (—); $[Mn_2OL_2]^{3+}$ generated by oxidation at +0.84 V vs SCE (— - —); $[Mn_2OL_2]^{4+}$ generated by oxidation at +1.3 V vs SCE (— — —). The visible part is represented in the insert for better accuracy.

In liquid SO_2 at −40 °C, the same compound is reported to exhibit two reversible one-electron processes at +0.89 V and +1.51 V/SCE, attributed to the formation of the Mn(III)Mn(IV) and Mn(IV)Mn(IV) species, respectively.

UV−Vis Spectroscopy. The electronic spectrum of $[Mn_2OL_2]^{2+}$ in acetonitrile (Figure 4) exhibits a broad band around 500 nm (ϵ = 1000 M^{-1} cm^{-1}) and a shoulder at 400 nm (ϵ = 4800 M^{-1} cm^{-1}). One intense band is also observed at 300 nm (ϵ = 21 000 M^{-1} cm^{-1}). Because no other spectra of Mn(III)-O−Mn(III) have been reported, comparison can only be made with compounds containing the dimanganese-μ-oxo-bis(μ-acetato) core. Above 450 nm, in $[Mn_2OL_2]^{2+}$ only one band is detected, whereas the μ-oxo-bis(μ-acetato) complexes as $[Mn_2O(O_2CCH_3)_2(TACN)_2]^{2+}$ present at least four transitions at 495 nm (ϵ = 324 M^{-1} cm^{-1}), 520 nm (250), 665 nm (95), and 910 nm (40).[47] This simplification of the visible spectrum when the M(III)−O−M(III) angle opens has already been observed with M = Fe.[48,49] This establishes a striking analogy between spectra of complexes containing the unit M(III)−O−M(III) for M = Mn and Fe.[50]

UV−vis spectroelectrochemistry of a solution 0.5 mM $[Mn_2OL_2]^{2+}$ is shown in Figure 4. Upon oxidation at 0.84 V/SCE the absorption spectrum changes drastically. A broad absorption band (ϵ = 3040 M^{-1} cm^{-1}) centered at 570 nm appears. This band is likely to be attributed to the phenolate → Mn(IV) charge-transfer band (LMCT) as reported for the $[Mn^{IV}$(1,4,7-tris(5-*tert*-2-hydroxybenzyl)-1,4,7-TACN)$]^+$ cation,[51] in which the intense band observed at 640 nm (ϵ = 7070 M^{-1} cm^{-1}) is attributed to a charge transfer (CT) between the phenolate residue and the Mn(IV). A comparison with $Mn_2O_2(salpn)_2$[18] for which the LMCT band is observed at 500 nm with ϵ = 7000 M^{-1} cm^{-1} is better, because $Mn_2O_2(salpn)_2$ contains a salicylidene-amino group identical with that found in $[Mn_2OL_2]^{3+}$. In $[Mn_2OL_2]^{3+}$, two other bands appear in the UV region at 408 nm (ϵ = 6970 M^{-1} cm^{-1}) and 344 nm (ϵ = 12 400 M^{-1} cm^{-1}). These bands are similar to those obtained in [Mn(III)Mn(IV)O_2(bispicen)$_2$]$^{3+}$.[52] Their relatively high intensity suggests that they are likely to be attributed to oxo → Mn(IV) CT transition. Besides, in the bispicen complex, this attribution is supported by the observation of an increase of the intensity of these bands when changing from the Mn(III)Mn(IV) to the Mn(IV)Mn(IV) oxidation level.[52]

Upon oxidation at 1.3 V/SCE, the broad band at 570 nm (ϵ = 3040 M^{-1} cm^{-1}) shifts at 710 nm (ϵ = 2500 M^{-1} cm^{-1}). Another well-defined band appears at 400 nm (ϵ = 10 698 M^{-1} cm^{-1}). This type of intense absorption band has been reported as the fingerprint of the formation of a phenoxyl radical rather than a metal-centered oxidation[19] in an Fe(III) monomer with ligand of the 1,4,7-tris(*o*-hydroxybenzyl)-1,4,7-TACN type.

Resonance Raman. As said above, we observed by spectroelectrochemistry at room temperature that upon oxidation at 1.3 V/SCE, a band appeared at 400 nm. It disappeared within 10 min, and we then suspected the formation of an unstable phenoxyl radical in place of a metal-centered oxidation. To be studied spectroscopically, the oxidized species $[Mn_2OL_2]^{4+}$ was prepared by controlled potential electrolysis at 1.2 V/SCE of $[Mn^2OL_2]^{3+}$ at −35 °C in acetonitrile. Following the advancement of electrolysis by coulometry, it was checked that the whole $[Mn_2OL_2]^{3+}$ complex was oxidized without any degradation. A color change from dark blue to deep green was observed. UV−vis spectroscopy of the final solution gave again the optical absorption feature at 400 nm, which is likely the signature of the phenoxyl radical.

Further evidence supporting the existence of a phenoxyl radical was obtained from resonance Raman spectroscopy (RR). Figure 5 shows the low-temperature RR spectra of the complex, excited using 413.1 nm light at various steps of the electrolysis. Bands are observed at 1540 cm^{-1}, 1572 cm^{-1}, 1605 cm^{-1}, 1630 cm^{-1} in RR spectra (Figure 5a and b) of the $[Mn_2OL_2]^{2+}$ and $[Mn_2OL_2]^{3+}$ complexes, respectively. The bands at 1572 cm^{-1} and 1605 cm^{-1} are attributed to the pyridine groups of the ligand[53] and the band at 1630 cm^{-1} to the Schiff base ligand vibration ν_{CN}.[54] The most dramatic changes in the RR spectrum occurred for the $[Mn_2OL_2]^{4+}$ complex (Figure 5c) as shown by the appearance of new bands at 1500 and 1620 cm^{-1} in addition to those mentioned above which are slightly shifted. The new bands are associated with the same species giving rise to the 400 nm absorption band in Figure 4 and are resonance enhanced at the 413.1 nm Raman excitation used here. These bands are characteristic vibrational signatures of phenoxyl radicals.,[20,55−57] They are assigned, respectively, to the C−O stetching (ν_{7a}) and

(48) Holz, R. C.; Elgren, T. E.; Pearce, L. L.; Zhang, J. H.; O'Connor, C. J.; Que, L., Jr. *Inorg. Chem.* **1993**, *32*, 5844−8850.
(49) Nivorozhkin, A. L.; Anxolabéhère-Mallart, E.; Mialane, P.; Davydov, R.; Guilhem, J.; Césario, M.; Audière, J.-P.; Girerd, J.-J.; Styring, S.; Schüssler, L.; Séris, J.-L. *Inorg. Chem.* **1997**, *36*, 846−853.
(50) Que, L., Jr; True, A. E. *Prog. Inorg. Chem.* **1990**, *38*, 97−184.
(51) Auerbach, U.; Weyhermüller, T.; Wieghardt, K.; Nuber, B.; Bill E.; Butzlaff, C.; Trautwein A. X. *Inorg. Chem.* **1993**, *32*, 508−519.
(52) Goodson, P. A.; Aderemi R. O.; Glerup, J.; Hodgson, D J. *J. Am. Chem. Soc.* **1990**, *112*, 6248−6254.
(53) Lin-Vien, D.; Colthup, N. B.; Fateley, W. G.; Grasselli, J. G. *The Handbook of Infrared and Raman Characteristic Frequencies of Organic Molecules*; Academic Press: New York, 1991; p 297.
(54) Carrano, C. J.; Carrano, M. W.; Sharma, K.; Backes, G.; Sanders-Loehr, J. *Inorg. Chem.* **1990**, *29*, 1865−1870.
(55) Tripathi, G. N. R.; Schuler, R. H. *J. Phys. Chem.* **1988**, *92*, 5129−5133.

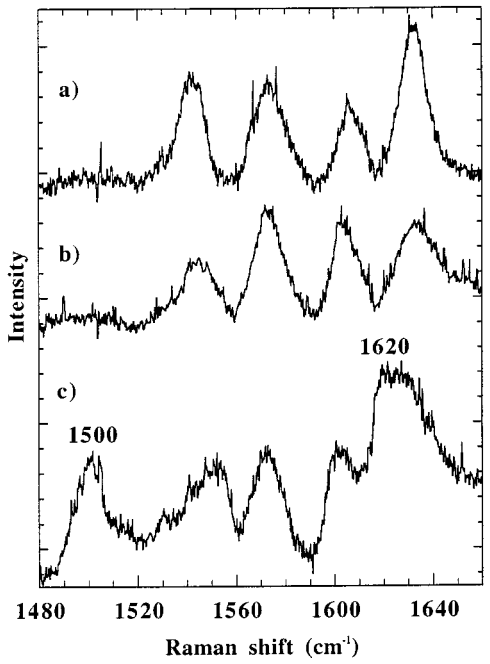

Figure 5. RR spectra of (a) $[Mn_2OL_2]^{2+}$ in acetonitrile, with 0.1 M $TBAClO_4$, taken at 15 K (λ_{exc} = 413.1 nm); (b) $[Mn_2OL_2]^{3+}$ in acetonitrile, with 0.1 M $TBAClO_4$, same conditions, obtained by oxidation at +0.84 V/SCE at −35 °C; (c) $[Mn_2OL_2]^{4+}$ in acetonitrile, with 0.1 M $TBAClO_4$, same conditions, obtained by oxidation at +1.3 V/SCE at −35 °C.

C−C stetching (ν_{8a}) vibrations of the phenoxyl radical.[20,55−58] The difference ($\nu_{8a} - \nu_{7a}$) is about 120 cm^{-1}, and the RR intensities ratio of the modes ν_{8a} and ν_{7a} appears to be ≥ 1, which suggests the phenoxyl coordination to the metal.[20] We have also obtained RR spectra of the complex containing deuterated phenolate groups. However this complex was fluorescent under the 413.1 nm exciting conditions and resulted in RR spectra with a reduced signal-to-noise ratio. Despite this interference we were able to clearly observe the most intense RR bands shifted toward lower frequencies at 1486 and 1591 cm^{-1} for the complex oxidized at 1.3 V/SCE. Similar shifts upon deuteration have been observed by RR[57,59] and IR.[60]

EPR Spectroscopy. The $[Mn_2OL_2]^{3+}$ species can be obtained in solution either by electrochemical preparation or by addition of a drop of H_2O_2 directly into a solution of $[Mn_2OL_2]^{2+}$. EPR spectra of $[Mn_2OL_2]^{3+}$ were recorded in both cases at 10 K in acetonitrile, and in both cases a very similar 18-line spectrum was observed. Figure 6 shows the spectrum recorded with a solution of $[Mn_2OL_2]^{3+}$ obtained electrochemically. This spectrum was simulated with rhombic tensors, with their principal axes taken parallel. We found $|A_{1x}| = 160 \times 10^{-4}$ cm^{-1}; $|A_{1y}| = 130 \times 10^{-4}$ cm^{-1}; $|A_{1z}| = 91 \times 10^{-4}$ cm^{-1}; $|A_{2x}| = 62 \times 10^{-4}$ cm^{-1}; $|A_{2y}| = 59 \times 10^{-4}$ cm^{-1}; $|A_{2z}| = 62 \times 10^{-4}$ cm^{-1}; $g_x = 2.006$; $g_y = 1.997$; $g_z = 1.982$ ($g_{iso} = 1.995$).[61] The agreement factor was $R = 4\%$. It is evident that the Mn center with the largest hyperfine values is the most anisotropic and that the center with the smallest hyperfine values is close to isotropy. The large anisotropy is typical for a Mn(III) ion and the isotropy corresponds to a Mn(IV) ion. The g-anisotropy is large ($g_x - g_z = 0.024$) as is the rhombicity [$(g_x - g_y)/(g_y - g_z) = 0.6$]. For the spin-doublet ground state of a strongly antiferromagnetic Mn(III)Mn(IV) pair, one has $[g] = 2\,[g^{III}] - [g^{IV}]$.[68] Mn(IV) is close to isotropy so that the anisotropy of $[g]$ mainly reflects that of $[g^{III}]$. The rhombicity of $[g]$ can thus be related to the symmetry around Mn(III) being far from axiality. In terms of wave function, this rhombicity around Mn(III) corresponds to the fact that the MO containing the fourth unpaired electron on Mn(III) is a mixture of d_{z^2} and $d_{x^2-y^2}$ orbitals, the x, y, and z axes being directed toward the ligands. Abragam and Bleaney[62] expressed this orbital as $\cos(\delta)\, d_{z^2} + \sin(\delta)\, d_{x^2-y^2}$ and computed the $[g^{III}]$ tensor as a function of the mixing angle δ and the ratio λ/Δ of the spin−orbit coupling constant to the crystal field splitting of the d orbitals in octahedral symmetry. Assuming $[g^{IV}]$ is isotropic, it is possible to extract the parameters g^{IV}, δ, and λ/Δ from the $[g]$ tensor of the pair.[63] Using this method, we found for the MO the composition $0.984\, d_{z^2} + 0.179\, d_{x^2-y^2}$ (see below for comparison with MO calculation).[64] Although this mixing seems weak, the g anisotropy is very sensitive to it. For instance, the maximum rhombicity would correspond to $0.956\, d_{z^2} + 0.259\, d_{x^2-y^2}$ ($\delta = 15°$) and an axial symmetry compressed along x, to $0.866\, d_{z^2} + 0.5\, d_{x^2-y^2}$ ($\delta = 30°$).

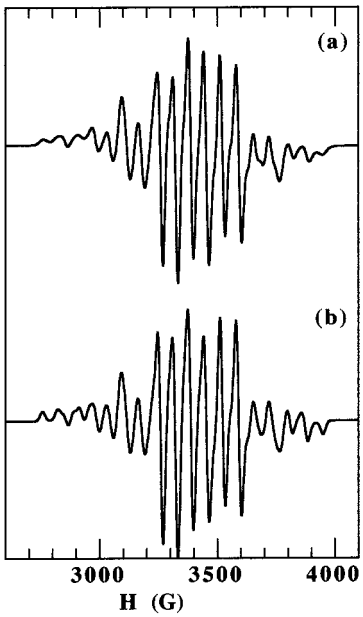

Figure 6. X-band EPR spectrum of $[Mn_2OL_2]^{3+}$ obtained electrochemically in acetonitrile. Spectrometer setting: modulation amplitude, 9.65 G; T = 10 K; ν = 9.434101 GHz. (a) experimental spectrum; (b) simulated spectrum. $|A_{1x}| = 160 \times 10^{-4}$ cm^{-1}; $|A_{1y}| = 130 \times 10^{-4}$ cm^{-1}; $|A_{1z}| = 91 \times 10^{-4}$ cm^{-1}; $|A_{2x}| = 62 \times 10^{-4}$ cm^{-1}; $|A_{2y}| = 59 \times 10^{-4}$ cm^{-1}; $|A_{2z}| = 62 \times 10^{-4}$ cm^{-1}; $g_x = 2.006$; $g_y = 1.997$; $g_z = 1.982$.

(56) Johnson, C. R.; Ludwig, M.; Asher, S. A. *J. Am. Chem. Soc.* **1986**, *108*, 905.
(57) Tripathi, G. N. R.; Schuler, R. H. *J. Chem. Phys.* **1984**, *81*, 113−121.
(58) Zurita, D.; Gautier-Luneau, I.; Menage, S.; Pierre, J.-L.; Saint-Aman, E. *J. Biol. Inorg. Chem.* **1997**, *2*, 46−55.
(59) Beck, S. M.; Brus, L. E. *J. Chem. Phys.* **1982**, *76*, 4700−4704.
(60) Hienerwaedel, R.; Boussac, A.; Breton, J.; Diner, B. A.; Berthomieu, C. *Biochemistry* **1997**, *36*, 14712−14723.
(61) The *x*, *y*, and *z* axes are a priori different from those mentionned later in the section on molecular orbital calculation.
(62) Abragam, A.; Bleaney, B. *Electron Paramagnetic Resonance of Transition Ions*; Oxford University Press: New York, 1970.
(63) Horner, O.; Charlot, M.-F.; Boussac, A.; Anxolabéhère-Mallart, E.; Tchertanov, L.; Guilhem, J.; Girerd, J.-J. *Eur. J. Inorg. Chem.* **1998**, 721−727.
(64) The values $g^{IV} = 1.991$ and $\lambda/\Delta = 0.0018$ were found. The g^{IV} value is acceptable and the λ/Δ one is likely related to a sizable covalency effect. See the previous reference for discussion of these points.
(65) C. Mathonière, Ph.D. Thesis, Université Paris-Sud, 1993.
(66) Perrée-Fauvet, M.; Gaudemer, A.; Bonvoisin, J.; Girerd, J.-J.; Boucly-Goester, C.; Boucly, P. *Inorg. Chem.* **1989**, *28*, 3533−3538.
(67) Blondin, G.; Girerd, J.-J. *Chem. Rev.* **1990**, *90*, 1359−1376.
(68) Zheng, M.; Khangulov, S. V.; Dismukes, G. C.; Barynin, V. V. *Inorg. Chem.* **1994**, *33*, 382−387.

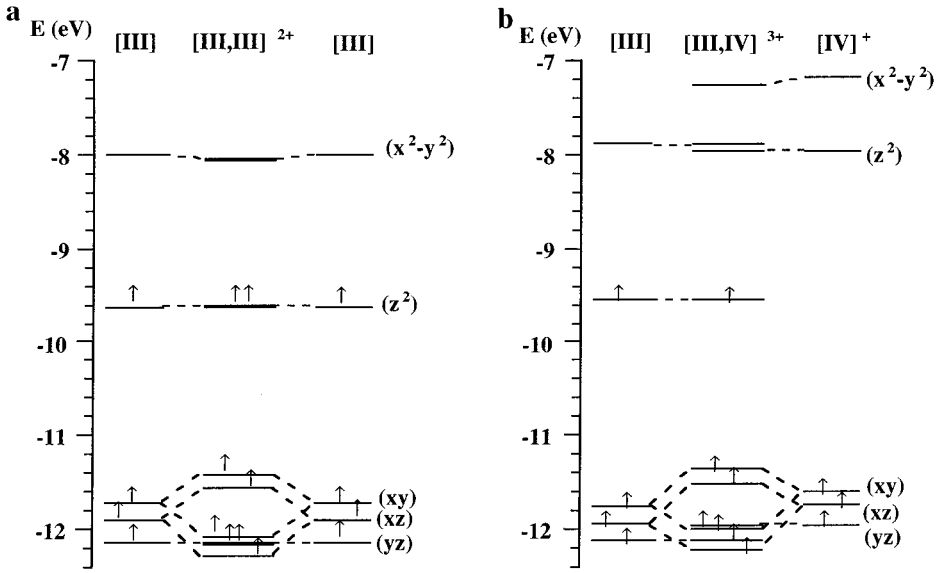

Figure 7. (a) Molecular orbital diagram for the model complex $[(NH_3)_4(OH)MnOMn(OH)(NH_3)_4]^{2+}$. The MOs are constructed from the highest energy single occupied orbitals of the monomeric fragment $[(NH_3)_4(OH)MnO]$, the so-called magnetic orbitals which are labeled by the majority d component. (b) Molecular orbital diagram for the model complex $[(NH_3)_4(OH)MnOMn(OH)(NH_3)_4]^{3+}$. The MOs are constructed from the orbitals of the fragments $[(NH_3)_4(OH)MnO]$ and $[OMn(OH)(NH_3)_4]^{2+}$.

The isotropic averages of the hyperfine tensors are $|A_{1iso}| = 127 \times 10^{-4}$ cm^{-1} and $|A_{2iso}| = 61 \times 10^{-4}$ cm^{-1}. These values are different from those observed in the case of the Mn(III)-O_2Mn(IV) units. For instance the EPR spectrum of $[Mn_2O_2(tren)_2]^{3+}$ was simulated with $|A_{1x,y}| = 150 \times 10^{-4}$ cm^{-1}; $|A_{1z}| = 128 \times 10^{-4}$ cm^{-1}; $|A_2| = 69 \times 10^{-4}$ cm^{-1}; $g_\perp = 1.961$; $g_\parallel = 1.953$.[65] This corresponds to $|A_{1iso}| = 143 \times 10^{-4}$ cm^{-1}. We have no clear explanation for the variations in isotropic coupling on Mn(III) from the typical value of 143×10^{-4} cm^{-1} to 127×10^{-4} cm^{-1} in $[Mn_2OL_2]^{3+}$. This can be either a local effect, because more spin density is transferred to the ligand in $[Mn_2OL_2]^{3+}$ than in $[Mn_2O_2(tren)_2]^{3+}$, or because the valence III is delocalized on both centers, which tends to average the isotropic couplings.[66] This last hypothesis is not favored for several reasons. Delocalization tends to reduce antiferromagnetism by double-exchange effects[67] and $[Mn_2OL_2]^{3+}$ was found to be strongly antiferromagnetic (AF). Structurally, as noticed above, both Mn ions in $[Mn_2OL_2]^{3+}$ are vastly different. Finally, the differences in hyperfine anisotropy around both Mn centers also favors strongly localized valencies. It thus seems more likely that some spin density is transferred to the phenoxy ligand.

The EPR spectrum of $[Mn_2OL_2]^{3+}$ shows that the 16-line paradigm, which is related to large AF exchange coupling and low anisotropy, can be overcome by a large rhombic anisotropy. A different case of deviation from the 16-line pattern for the EPR spectrum of Mn(III)Mn(IV) pair, related to a weak exchange coupling, has been identified by Zheng et al.[68]

The deep-green solution of $[Mn_2OL_2]^{4+}$ obtained by electrolysis at −35 °C in acetonitrile gives no EPR spectrum at 10 K. This could be due to a strong coupling between the $S = {}^1/_2$ spin of the Mn(III)Mn(IV) core and that of the phenoxyl radical.

Simple Theoretical Considerations on the Electronic Structure of $[Mn_2OL_2]^{2+}$ and $[Mn_2OL_2]^{3+}$. Extended Hückel calculations of the molecular orbitals of structural models $[(NH_3)_4(OH)MnOMn(OH)(NH_3)_4]^{2+}$ or $^{3+}$ of $[Mn_2OL_2]^{2+}$ and $[Mn_2OL_2]^{3+}$ were performed using the CACAO code.[69] The geometry deduced from X-ray crystallography was used but was idealized to C_{2h} and C_s for $[Mn_2OL_2]^{2+}$ and $[Mn_2OL_2]^{3+}$, respectively. Calculations were also performed on corresponding mononuclear fragments $[(NH_3)_4(OH)MnO]^0$ or $^+$. Molecular orbital energies for $[(NH_3)_4(OH)MnOMn(OH)(NH_3)_4]^{2+}$ and of its constitutive fragments $[(NH_3)_4(OH)MnO]^0$ are represented in Figure 7a. In the assembly of two such fragments to give the dimer, a O^{2-} group is eliminated, which leads to the 2+ charge. Inspection of the orbitals of a mononuclear Mn(III) fragment shows very clearly the large gap induced by the Jahn−Teller effect in the "e_g" type orbitals. The elongation along the N_{py}−Mn−N_{py} axis noticed in the structure analysis leads to the stabilization of an orbital pointing toward those N_{py} atoms because its metal d orbital composition is mainly d_{z^2}, although not purely. The molecular orbitals of the dinuclear assembly show perfectly that the MOs with the greatest splitting are those of the d_{xy} and d_{xz} type, *x* being the Mn−Mn axis. This is in complete agreement with the Dunitz−Orgel diagram for a M−O−M unit.[70] This corresponds to a π-type interaction mediated by p_y or p_z orbitals of the bridging oxygen atom. The other MOs have very weak splitting. Consequently, as expected, the AF coupling through the linear oxo bridge in $[Mn_2OL_2]^{2+}$ arises from the *xy* and *xz* interactions.[71]

Molecular orbital energies for $[(NH_3)_4(OH)MnOMn(OH)(NH_3)_4]^{3+}$ are represented in Figure 7b as those of corresponding moieties. The contraction of the coordination sphere around the Mn(IV) ion increases spectacularly the energy of the "e_g" type orbitals around Mn(IV): the energy of the d_{z^2}-rich MO is now close to −8 eV and that of the $d_{x^2-y^2}$ type MO close to −7 eV. Again the most efficient interactions are the *xz* and *xy*. This is at the origin of the large AF coupling in $[Mn_2OL_2]^{3+}$. As reported earlier,[71] the exchange coupling constant can be written as

$$J = (1/n_A n_B)\sum_{ij} J_{ij}$$

where J_{ij} is the interaction between orbitals i on metal A and j on metal B, $n_{A(B)}$ being the number of unpaired electrons on A

(69) Meali, C.; Proserpio, D. M. *J. Chem. Educ.* **1990**, *67*, 399−402.

(70) Dunitz, J. D.; Orgel, L. E. *J. Chem. Soc.* **1953**, 2594−2596.

(71) Hotzelmann, R.; Wieghardt, K.; Flörke, U.; Haupt, H.-J., Weatherburn, D. C.; Bonvoisin, J.; Blondin, G.; Girerd, J.-J. *J. Am. Chem. Soc.* **1992**, *114*, 1681−1697.

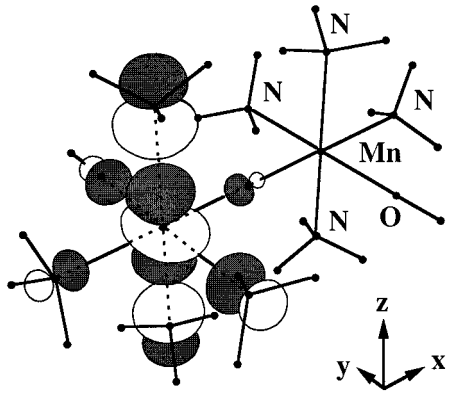

Figure 8. Highest energy molecular orbital containing one unpaired electron in $[(NH_3)_4(OH)MnOMn(OH)(NH_3)_4]^{3+}$. It is located around Mn^{III}. Atoms are indicated on the Mn^{IV} side only, for clarity.

or B. Considering that the *xz* and *xy* pathways are the only ones implied, it can be written

$$J = (1/n_A n_B)(J_{xy,xy} + J_{xz,xz})$$

From the experimental value of *J*, it can be deduced that $J_{xy,xy} + J_{xz,xz} = 4*4*(-216) = -3456\ cm^{-1}$ for $[Mn_2OL_2]^{2+}$. Assuming that taking one electron away from $[Mn_2OL_2]^{2+}$ induces no geometry variation important for the interactions between centers, we calculated for the coupling in $[Mn_2OL_2]^{3+}$, $J = -288\ cm^{-1}$. Experimentally we found $-353\ cm^{-1}$, which indeed indicates a stronger AF coupling in $[Mn_2OL_2]^{3+}$ than in $[Mn_2OL_2]^{2+}$, but the experimental value is 22% larger in absolute value than the simple previous guess. The trend is correct, but the geometrical rearrangements induced by the oxidation clearly cannot be ignored.

The highest energy molecular orbital containing one unpaired electron in $[(NH_3)_4(OH)MnOMn(OH)(NH_3)_4]^{3+}$ is represented in Figure 8. Its metal composition contains a major d_{z^2} contribution but also a $d_{x^2-y^2}$ one. It is centered on the Mn(III) ion. Two features of the electronic structure of the Mn(III)Mn(IV) complex can be understood from the nature of this orbital: (i) the localization of the valencies; (ii) the nonaxial anisotropy. For the first characteristic, we notice that this orbital has its main component perpendicular to the Mn−Mn axis so that its overlap with its corresponding partner on the other Mn center is very poor. The transfer integral β between these two orbitals is thus very small; this is precisely the origin of the electron localization. This weak delocalization energy cannot overcome the trapping energy because of the rearrangement of the coordination sphere related to electron transfer.[67] For the second feature, the rhombicity, the orbital of Figure 8 can be compared with that containing the fourth unpaired electron on Mn(III), the composition of which was deduced from EPR. If one takes into account normalization, the composition is $0.988\ d_{z^2} + 0.154\ d_{x^2-y^2}$ in good agreement with what has been found by EPR. Moreover, this suggests that the principal axes of the spin Hamiltonian tensors are close to the axes used in the MO calculation.

Discussion

In this work we have prepared a Mn dinuclear species with a ligand containing a phenolate group. We showed that this species could be prepared in three oxidation states $[Mn_2OL_2]^{2+,3+,4+}$. The 2+ species was identified as Mn(III)Mn(III) and the 3+ as Mn(III)Mn(IV). Surprisingly, oxidation to the 4+ species was found to implicate not a Mn ion but a phenolate group, to give a $[Mn^{III,IV}{}_2OLL^{\circ}]^{4+}$ species.

Is the radical bound to the Mn(III) or the Mn(IV) ion? It is difficult to answer this question experimentally, although it seems likely that the oxidized phenolate is that linked to Mn(III). Magnetization experiments could contribute to solving this problem because the electronic spin value for the ground state must depend on the topology of the spin system.

Why in this complex does the second oxidation take place on one phenolate and not on a Mn ion? We have previously stressed the important gap in potential between the two redox processes Mn(IV)Mn(IV)/Mn(IV)Mn(III) and Mn(IV)Mn(III)/Mn(III)Mn(III) in Mn_2O_2 systems, this gap being approximately 1 V in acetonitrile.[72] We have proposed that this value mainly reflects an electron−electron repulsion term in the Mn(III)Mn(III) state (Mn−Mn distance, 2.7 Å) which disappears in the higher oxidation states.[72] Electron−electron repulsion energy is inversely proportional to the metal−metal distance so that the difference in redox potentials for the linear unit Mn−O−Mn unit (Mn−Mn distance, 2.7 Å) can be estimated to be $1*2.7/3.5 = 0.77$ V. The oxidation of the $[Mn^{III,IV}{}_2OL_2]^{3+}$ complex to the Mn(IV)Mn(IV) state would then need a potential of approximately $0.54 + 0.77 = 1.31$ V/SCE, a calculation neglecting the changes in solvation energy which must be small because of the bulkiness of the complex. It thus simply turns out that this redox potential is higher than that of a phenolato group.

This study confirms the difficulty of storing two positive charges on the two metal ions of a di-μ-oxo or mono-μ-oxo unit in a narrow potential range. One way to circumvent this difficulty is to use one metal ion and a redox-active ligand as here. Another possibility is to couple the first oxidation to a deprotonation step which can bring the two successive oxidation steps close together as previously shown with $[Mn_2O_2(bpy)_4]^{3+}$.[73]

The very fact that the separation in potential of the two successive steps Mn(III)Mn(III) → Mn(III)Mn(IV) and Mn(III)Mn(IV) → Mn(IV)Mn(IV) is about 1 V in di-μ-oxo units and likely not much less in mono-μ-oxo units poses a problem for understanding the function of the OEC. Considering that the OEC is likely constituted by two such units, let us say $\{Mn^{III}Mn^{III}\}_A/\{Mn^{III}Mn^{IV}\}_B$, the first oxidation must be that of pair A with the potential $E^0{}_A$. This would lead to an S_1 state represented by $\{Mn^{III}Mn^{IV}\}_A/\{Mn^{III}Mn^{IV}\}_B$. In the OEC the potential of the S_1/S_0 transition is the lowest, as proven by oxidation of S_0 by $Tyr_D{}^{\circ}$.[74] The second step in such a scheme would likely consist in the oxidation of B and lead to $\{Mn^{III}Mn^{IV}\}_A/\{Mn^{IV}Mn^{IV}\}_B$ (state S_2). If the third step implicates the pair A, from what we said above, it must occur at approximately $E^0{}_A + 1$ V. However this potential must be lower than the potential of $Y_Z{}^{\circ}$ (≈1 V/NHE), which means that $E^0{}_A$ cannot have a value larger than 0 V/NHE which would be in contradiction with experiment.[74] One of the two solutions mentioned above for artificial systems could operate in nature. A redox active ligand could be oxidized in the $S_2 \rightarrow S_3$ step. Indeed, this has been proposed from XANES measurements.[2] An alternative could be a deprotonation of a ligand in the $S_0 \rightarrow S_1$ step. This would give a potential equal to $E^0{}_A + 0.06\ pK_a{}^{III,III}$, which could be not too different from the $E^0{}_A + 1$ V potential

(72) Anxolabéhère-Mallart, E.; Girerd, J.-J. *Spectroscopic Methods in Bioinorganic Chemistry*; ACS Series, in press.
(73) Thorp, H. H.; Sarneski, J. E.; Brudvig, G. W.; Crabtree, R. H. *J. Am. Chem. Soc.* **1989**, *111*, 9249−9250.
(74) Vass, I.; Styring, S. *Biochemistry* **1991**, *30*, 830−839.

in the step $S_2 \rightarrow S_3$. This deprotonation could implicate a hydroxo bridge as shown with model complexes by Baldwin and Pecoraro.[75] Indeed, it does not seem possible to store several positive charges on the metal ions of a metal polynuclear cluster without involving auxiliary chemical changes.

Conclusion

For the first time a Mn−O−Mn-containing complex has been fully characterized in three oxidation states. The ligand used was the pentadentate *N*,*N*-bis(2-pyridylmethyl)-*N*′-salicyliden-1,2-diaminoethane ligand. The compound **$[Mn_2OL_2](ClO_4)_2$** has been crystallized and its structure resolved. The structure of the $[Mn_2OL_2]^{2+}$ complex reveals a Jahn−Teller elongation along the $N_{py}-Mn-N_{py}$ axis. The visible absorption spectrum is considerably simpler than that of μ-oxo-bis(μ-acetato) Mn(III)-Mn(III) complexes. This confirms that several of the corresponding transitions imply an oxo-metal charge-transfer sensitive to the Mn−O−Mn angle. This has already been studied by Que and True for Fe(III)−O−Fe(III) entities.[50] The magnetic coupling in $[Mn_2OL_2]^{2+}$ has been found strongly AF, as expected from previous theoretical work.[71]

$[Mn_2OL_2]^{2+}$ can be oxidized electrochemically to $[Mn_2OL_2]^{3+}$ at $E_1^{1/2} = 0.54$ V/SCE and to $[Mn_2OL_2]^{4+}$ at $E_2^{1/2} = 0.99$ V/SCE. Crystals of **$[Mn_2OL_2](ClO_4)_{2.37}(PF_6)_{0.63}$** have been grown and the structure has been resolved. It offers an opportunity to compare the same complex in two different oxidation states. The structure shows a 0.2-Å contraction of the $N_{py}-Mn$ bonds as a consequence to the oxidation of the metal. The Mn−Mn distance is slightly changed, and the oxo atom is displaced by only 0.03 Å from the center position. The one-electron oxidation of $[Mn_2OL_2]^{2+}$ induces a spectacular change in the UV−vis absorption spectrum. A broad and intense band peaking at 570 nm appears corresponding to a phenolate → Mn(IV) transition. The EPR spectrum of $[Mn_2OL_2]^{3+}$ shows 18 lines and has been analyzed with a hyperfine tensor deviating from axiality on Mn(III), an almost isotropic one on Mn(IV) and a rhombic [*g*] tensor. This rhombicity has been related to the low-symmetry Mn(III) site. Exchange coupling in $[Mn_2OL_2]^{3+}$ has been found more strongly AF than in $[Mn_2OL_2]^{2+}$. Molecular orbital calculations show that the excess unpaired electron is localized on one center in an orbital with a dominant d_{z^2} component pointing perpendicularly to the Mn−Mn axis. This leads to a poor overlap with its partner on the other Mn atom and thus explains the localized valencies. The presence of a phenoxyl radical in the most oxidized species $[Mn_2OL_2]^{4+}$ was evidenced by RR spectroscopy.

The relatively small separation in redox potentials (0.45 V) observed here between the two successive oxidations is related to the fact that the first oxidation concerns one Mn ion whereas the second oxidation occurs at one of the phenolate groups. This confirms the difficulty to store two positive charges on Mn in a narrow range of potential in Mn clusters.

The redox potentials for the two oxidations of this complex are well adapted to oxidation by $Ru(bpy)_3^{3+}$ to test the possibility of coupling between an artificial charge-separation system using light on one hand and a Mn artificial charge storage device on the other with a phenol group as a relay. Experiments are being conducted in this respect.

Acknowledgment. This work has been supported in part by the European Training and Mobility of Researchers "Ru-Mn Artificial Photosynthesis" program. We thank Drs. Katja Berg and Catherine Berthomieu for stimulating discussions on the manuscript.

Supporting Information Available: Atomic coordinates, equivalent isotropic displacement parameters, anisotropic displacement parameters and bond lengths and angles for **$[Mn_2OL_2](ClO_4)_2$** and **$[Mn_2OL_2](ClO_4)_{2.37}(PF_6)_{0.63}$**. This material is available free of charge via the Internet at http://pubs.acs.org.

IC980832M

(75) Baldwin, M. J.; Pecoraro, V. L. *J. Am. Chem. Soc.* **1996**, *118*, 11325−11326.